https://africanjournalofbiomedicalresearch.com/index.php/AJBR
Afr. J. Biomed. Res. Vol. 27(6s) (December 2024);17 - 25
Research Article

Thermally Curable Cresol Based Polyureathane: Synthesis, Characterization And Anticorrosive Properties

C. Usha[1*], M. Sivaraju[2]

[1,2]Department of Chemistry, Thiruvalluvar Government Arts College,
Affiliated to Periyar University, Rasipuram, Namakkal-637401, Tamilnadu, India

***Corresponding Author:** C. Usha
*Email: tkr_jai@hotmail.com

Abstract
Extensive research has been conducted to address the issue of corrosion in steel applications for industrial purposes and other fields. This study introduces a polyurethane-based material utilizing benzoxazine as a monomer, which has undergone thorough characterization through NMR, UV-visible, and FT-IR spectroscopic methods. The electronic properties of the synthesized monomer have been elucidated through DFT analysis, including FMO analysis and molecular mapping studies. Furthermore, different ratios of polyurethane precursor have been employed to produce an anti-corrosive co-polymer material revealing its hygroscopic nature and gel formation. The Tafel experiment was also conducted to evaluate the activity of the coated polymer, demonstrating its superior performance compared to bare mild steel.

Keywords: Simple monomer, Co-polymer, Corrosion studies, DFT and MEP.

***Author for correspondence: Email:** tkr_jai@hotmail.com*

Received:30-11-2024 *Acceptance: 08-12-2024*

DOI: https://doi.org/10.53555/AJBR.v27i6S.4890

Introduction

Industrial metals face a great deal of risk from corrosion, which affects both their overall safety and cost. There are now several strategies for preventing metal corrosion using organic/inorganic coatings, adding corrosion inhibitors, and adjusting the composition and smelting processes of metals[1-4]. The application of corrosion inhibitors is the most practical and economical choice among these. When it comes to the final features of objects made of metal, stone, wood, and polymers, surface quality is vital[5]. Almost all commercial items go through finishing processes to get the surface to the correct size, shape, or texture. One often-used method for this is abrasive machining, where the type of abrasive tool used has a big impact on the final result[6]. By making sure the tool is constructed and composed correctly, producers may produce the highest-quality surface layer[7]. Corrosion of mild steel (MS) is a significant problem across various industries such as petrochemical engineering, chemical processing, mining, industrial cleaning, and material refining. It can result in financial losses and pose health and safety risks in corrosive environments. Pipeline failures that carry natural gas, chemicals, and oil are mainly caused by external corrosion. Such pipeline damages can cost up to 3.4% of the world's gross domestic product, which amounts to around US $2.5 trillion (2013)[8]. Corrosive elements in the environment such as acidity in soils, water's oxygen and air oxygen, brine solution's carbon dioxide, lead or copper like

natural catalyst and concentrated salts are responsible for the damage caused to pipelines[9]. Organic coatings are commonly used to prevent corrosion in metals and steel. They act as barriers to the flow of electric current and prevent harmful substances from causing damage[10]. Resistant organic coating is a primary method of protecting mild steel from corrosion during industrial processes. The approach involves creating a barrier to stop corrosive agents from passing through, which is believed to be an economical and practical solution[11]. It was common practice to characterize a coating's protective barrier qualities using the rates of moisture and ion transport through its polymer network[12].

Various polymeric compounds have been utilized in this study to protect mild steel. One of these compounds is polybenzoxazines, a novel type of phenolic resins derived from benzoxazine through ring-opening polymerization[13]. The advantages of polybenzoxazines have garnered significant interest due to their ability to address the limitations of traditional phenolic resins. It is expected that polybenzoxazines will serve effectively as a thermoset resin in various fields, including electronics[14-17]. The primary challenges associated with polybenzoxazines are their high curing temperature requirement (approximately 200°C) and brittleness, which is a common issue with thermoset resins. Various catalysts have been explored to lower the polymerization temperature[18]. Polybenzoxazine has a notable drawback, which is its limited degree of polymerization. In order to enhance the performance of polybenzoxazine, various studies have been conducted on copolymers[19-22], polymer alloys[23], fiber-reinforced composites[24], and clay nanocomposites[25]. Additionally, another effective approach for enhancing performance is through the polymerization of novel monomers that contain different polymerizable groups, such as ethynyl, nitrile, propargyl and allyl groups[26].

Synthesis of the monomer

3-aminoacetophenone and O-cresol (1 g, 6.572 mmol) are the significant precursor for the synthesis of monomer. The reaction of these precursors with paraformaldehyde (0.414g) in the presence of 20 mL of chloroform at reflux condition yielded benzoxazole monomer. The completion of the reaction is monitored by thin layer chromatography and the final reaction mixture was extracted using chloroform (150mL), and washed with sodium hydroxide, water and brine solution. The chloroform layer is separated and dried over anhydrous sodium sulfate and the resulting chloroform solution was then evaporated under reduced pressure to obtain the monomer. The obtained monomer is directly taken for the coating of mild steel.

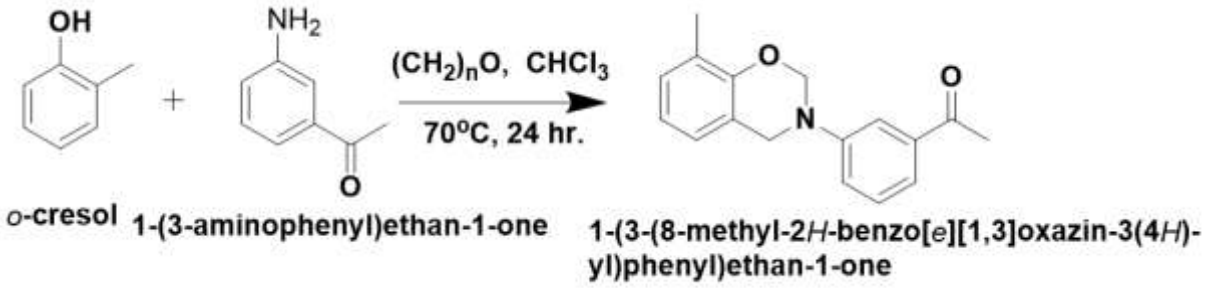

Scheme 1: Synthetic route for the benoxazine monomer

Synthesis of the anti-corrosive agent (polymer synthesis) [27]

The MS substrates were prepared for coating by first undergoing mechanical blasting to Sa $_{2.1/2}$ and then being cleaned in hexane, ethanol and acetone by wiping method. The coating of MS plate is achieved by dip coating followed by thermal curing. The monomer was dissolved in the mixture of 1,4-dioxane:toluene (7:3), with the various concentration of isocyanate hardener (CABz-PU 60, CABz-PU 80, or CABz-PU 100). After being left at room temperature for 10 min, the samples were dried for an hour in hot air oven to remove any remaining solvent molecules. Finally, the polymerization is achieved at 180°C for 2 hours in muffle furnace.

Water absorption studies

The water absorption capacity of the samples cured at a specific temperature was evaluated using the guidelines from the ASTM D570. After being cured and dried at 80^{o} C without any air, the samples were weighed to ensure they were completely dry. Subsequently, the sample was submerged in water at room temperature for 24 hours. After that, the samples were dried entirely using tissue paper and weighed once again. We calculated the percentage of water absorption using the following equation:

Percentage of water absorption = $[(W_a-W_b)/W_b] \times 100$

Where,

W_a = Weight of the cured sample after exposure to water absorption

W_b = Weight of the cured sample before exposure to water absorption.

Gel content studies

Similarly, all cured samples had their gel formation content checked after being immersed in xylene for a day at room temperature; prior to this, the weight of the bare sample was recorded. After that, a vacuum oven was used to dry all of the samples, and the following formulas were used to determine how much gel there was:

Percentage of gel content = (W_a/W_b) X 100
Where,
W_a = weight of cured coating samples after the extraction
W_b = weight of cured coating samples before the extraction

Computational calculations
The investigation into the chemical reactivity of the synthesized monomer was greatly enlightened by the study of Frontier Molecular Orbital (FMO) in DFT analysis. The entire DFT analysis was conducted using the Gaussian 09W software program. In relation to this investigation, the monomer's 3D structure was first optimized using 3D chem draw, which involved pasting the structure into Gaussian software and conducting an analysis utilizing the B3LYP/6.311 G basis set[28]. With the aid of the Gauss View software, the optimized structure could be seen and utilized for a variety of analytical tasks, including determining the electron density on the molecule and determining the molecular electrostatic potential.

Electrochemical studies
Tafel Polarization experiment[29]
By aid of these values, the corrosion efficacy was calculated using following formulae,
Corrosion rate = $\frac{Icorr \times K \times EW}{\rho A}$
Where,
K = Corrosion rate constant, 3272 mm/year,
EW = Equivalent weight 27.9 g
ρ = Material density, 7.85 g/cm³ for mild steel
A = Area of the sample, 1 cm²

Corrosion Efficiency (%) = $[\frac{Icorr(b)-Icorr(c)}{Icorr(b)}] \times 100$
Where,
$I_{corr(b)}$ = corrosion current values for the blank mild steel (without coating)
$I_{corr©}$ = corrosion current values for the coated mild steel

Results and discussion
Characterization of the monomer
^{1}H-NMR analysis
The nuclear magnetic resonance spectroscopy is an important and best tool to predict the perfect structure of the organic molecule. Henceforth, this analytic technique was used for the analysis of monomer. Chemically, the synthesized monomer contains 17 protons, which are present in different chemical environments. The ^{1}H-NMR spectrum in figure 1 displays all of these protons. Among them, there are four protons located in the -CH_2- groups attached to the benzoxazole ring. These protons are two separate singlet peaks at 4.9 and 5.3 ppm. Additionally, another singlet peak at a highly shielded region, specifically at 2.1 and 2.4 ppm, accounting for three protons each. These protons are associated with the methyl groups attached to the phenyl ring and ketone group, respectively. The remaining seven aromatic protons appear in the range of 6.7 to 7.4 ppm with multiple peaks, which confirms the chemical structure of the monomer.

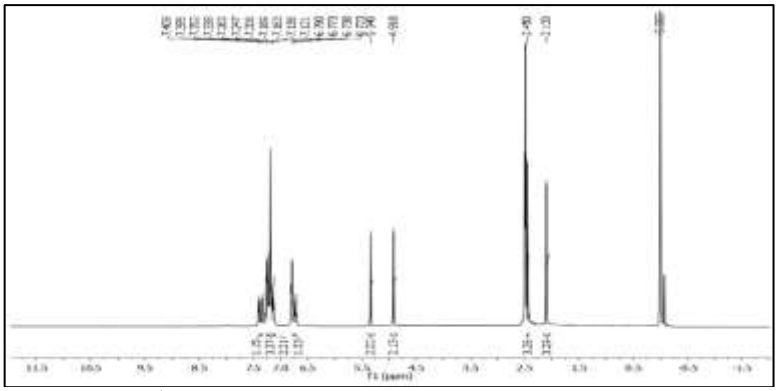

Figure 1: ^{1}H-NMR spectrum of the monomer in $CDCl_3$ solvent

FT-IR analysis
The significant functional groups of the monomer and polymers can be confirmed by Fourier-Transform infrared spectroscopy. The FT-IR spectrum of monomer and various combinations of polyurethane based polymers are represented in Figure 2. Various functional group present in polymer/monomer like C=O, C=C, C-N, C-O are confirmed by FT-IR spectrum. In the monomer, the characteristic peaks such as the aromatic C-H stretching vibrations are observed at 2928 cm^{-1} and 2862 cm^{-1} and the C-N stretching vibration is observed at 1143 cm^{-1}. The aliphatic stretching vibration is observed at 2954 cm^{-1}. Furthermore, the stretching vibrations for C-O-C are observed at 1235 cm^{-1}, 1209 cm^{-1} and 1091 cm^{-1}. The major characteristic frequency C=O is observed at 1686 cm^{-1} which is present in the phenylene unit. For instance, the amine unit appeared at 3337 cm^{-1} and methylene unit appeared at 3070 cm^{-1} respectively. The stretching vibrations for C-N and C-O-C bonds are observed at 1515 cm^{-1} and 1146 cm^{-1}, respectively. Additionally, the appearance of strong absorbance at 1636 cm^{-1} indicate the presence of C=O stretching vibrations, which is present in the polyurethane unit.

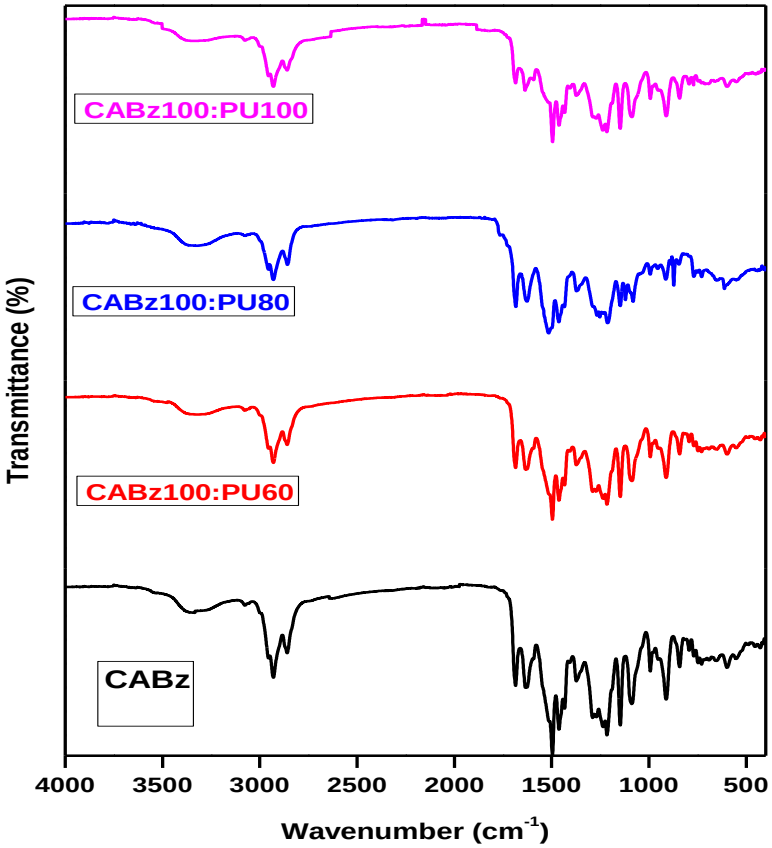

Figure 2: Solid state FT-IR spectra of monomer (A), and various ratio of polymeric composites such as 60 % (B), 80 % (C) and 100 % (D)

UV-visible spectroscopy

UV-visible spectroscopy analysis was performed on the synthesized monomer and its polymers by recording the spectra at room temperature using water as a solvent. Figure 3 depicts two distinct peaks of the synthesized monomer at 342 nm and 298 nm, representing the n-π* and π - π* electronic transitions. Moreover, the increasing concentration of polyurethane leads to red shift in the UV-Visible spectrum. Specifically, absorption peak is shifted to 20nm higher wavelength. These results highlight the significant impact of polyurethane on the characteristics of the monomer, suggesting that a material containing 100% polyurethane may offer maximum advantage in anti-corrosion procedure..

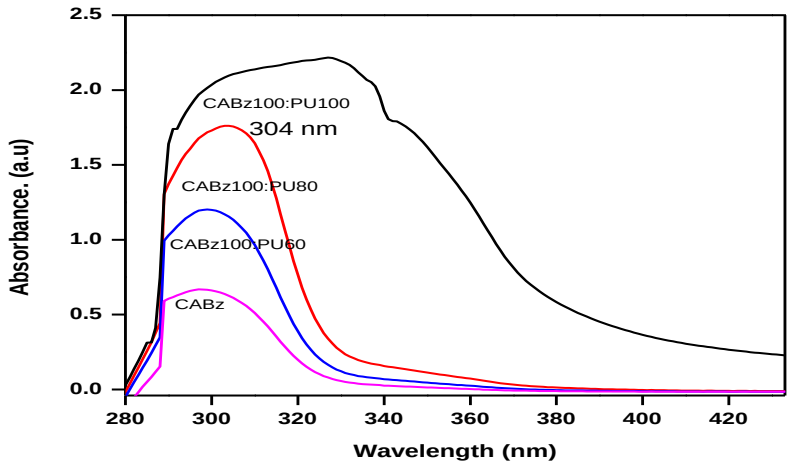

Figure 3: Absorption spectra of monomer (pink), and various ratio of polymeric composites such as 60 % (blue), 80 % (red) and 100 % (black) in solution state at room temperature..

Tafel experiments

In figure 4, we observe the Tafel plot utilized for determining the corrosion current and potential of the synthetic polymeric material. Estimating the corrosion current density involved superimposing a straight line over the linear component of the anodic and cathodic curves using the corrosion potential. These characteristics significantly impact the corrosion behavior of artificial materials. Typically, materials with higher conductivity and more electrons exhibit accelerated corrosion. Conversely, materials with a higher positive corrosion potential corrode at a slower pace. Consequently, polymeric materials necessitate a higher potential to showcase their conductivity.

The studies on corrosion of co-polymeric materials have been carried out using electrochemical methods such as the Tafel experiment. The outcomes were compared with a steel plate that was left untreated as a blank, and the estimated parameters are presented in table 1. The blank had a higher corrosion current value of 15.77 µA, which can be significantly reduced by increasing the concentration of the polyurethane-containing polymer. A minimum current value for corrosion was found to be 0.12 µA for the highest concentration of polyurethane. This indicates that synthesized co-polymers considerably reduce the formation of rusted iron on the surface of steel plates in comparison to untreated plates. In this study, it was found that the synthesized co-polymer has a positive potential, which means that the polyurethane part of the polymer has a lower negative potential. This indicates that polyurethane can form strong chemical bonds with monomers, which can prevent iron oxidation and protect against air molecules. The effectiveness of this polymer against corrosion was measured using I_{corr}, and it was found that the blank had a corrosion rate of 183391.54 millimeters per year (mmpy), which was reduced up to 110 times with the highest content of the polymer. The efficiency of the material in this line is also evaluated, with the PU component reaching an impressive improvement of 99% when it constitutes 100% of the material, compared to 60% PU. Additionally, the polarization resistance clearly demonstrates the positive impact of PU on the polymeric materials, resulting in a resistance that is 15 times higher. Taking into account all the parameters calculated from the Tafel plot, it is highly recommended to utilize the synthesized materials as an anti-corrosive agent for mild steel, as it is expected to be more effective.

Table 1: The parameter obtained from the electrochemical experiment.

Sample (APB:PU)	Icorr (µA)	Ecorr (mV)	Corrosion Rate (mmpy)	Polarization resistance (KΩ*cm²)	Corrosion inhibition Efficiency (%)	Tafel Constant (mV/dec)	
						βa	βc
Blank	15.77	-828.0	183391.54	2.02	0.00	235.3	190.6
100:60	7.28	-638	84660.14	5.02	53.83	-179	159
100:80	0.23	-534	2674.70	10.1	98.54	-15.1	8.7
100:100	0.12	-508	1395.49	30.6	99.23	-23.1	13.2

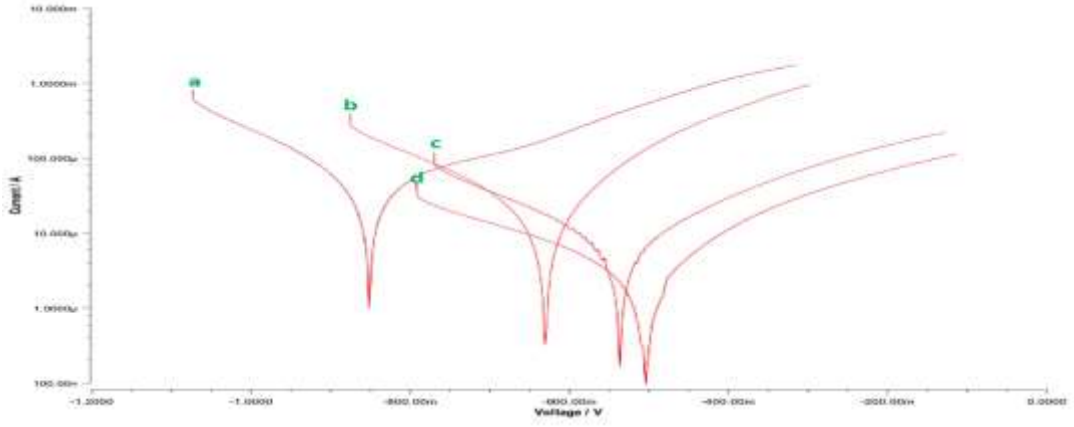

Figure 4: Tafel experiment of the (a) blank and various concentrations of poly-urethane materials (b) – 60 %, (c) – 80 % and (d) – 100 %)

Water adsorption and gel content studies

Water diffusion studies in polymeric corrosion materials are vital and may differ depending on the branching and cross-linkage density of the polymeric materials. The cross or breach density determines the effectiveness of the binder during coating leads to greater hydrogen bonding with the materials[29]. The water adsorption capacity of the monomer and its polymer was examined, yielding a better result, as shown in figure 5. In the gel content analysis, the monomer accounted for just a small portion of the water adsorption. This demonstrates that the monomer may be highly hydrophobic, and clearly, polyurethane will improve its co-polymeric nature. The data clearly reveals a reciprocal connection with polyurethane concentration, with greater concentrations yielding a relatively low percentage of water adsorption (0.75%). These findings are substantially correlated with gel content, indicating that it has a promising physical character that could be used for corrosion investigations. As a result, the gel content of the synthesized monomer and polymeric material was

assessed, and the data are presented in figure 6. The monomer alone has a higher gel content of 87%, which is further increased by the production of a co-polymer with polyurethane. The gel content is continually raised by increasing the amount of polyurethane substance until finally, it achieved 94% gel content with an equal quantity of polyurethane and monomer. These results could be attributed to the presence of a very intricate polymeric network created by the polyurethane, which could result in a denser bonding structure. Co-polymerization with polyurethane is an essential aspect of this study; thus, it might be assumed that increasing concentrations of polyurethane attributes to be the best anti-corrosive agent.

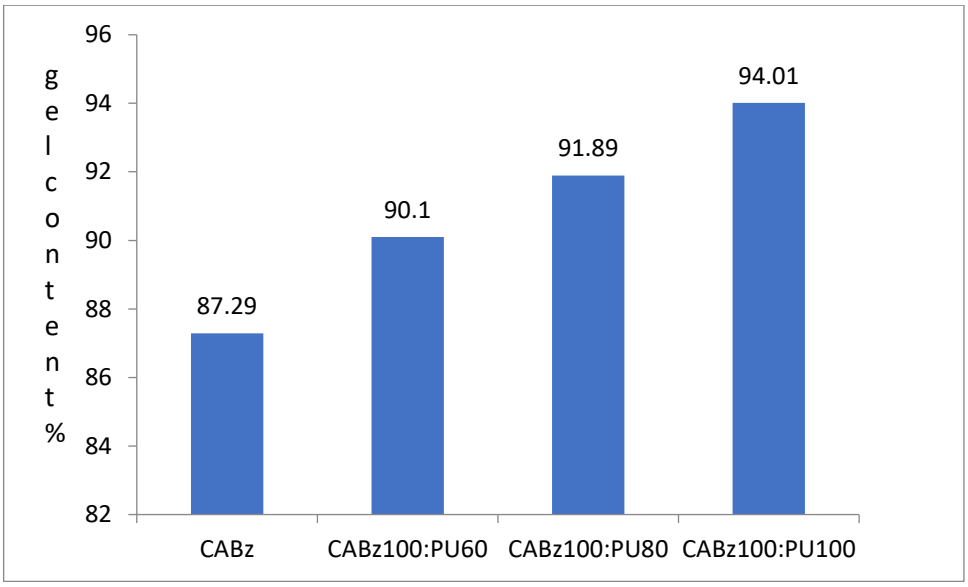

Figure 5: The percentage of gel content analysis of monomer and its co-polymeric material.

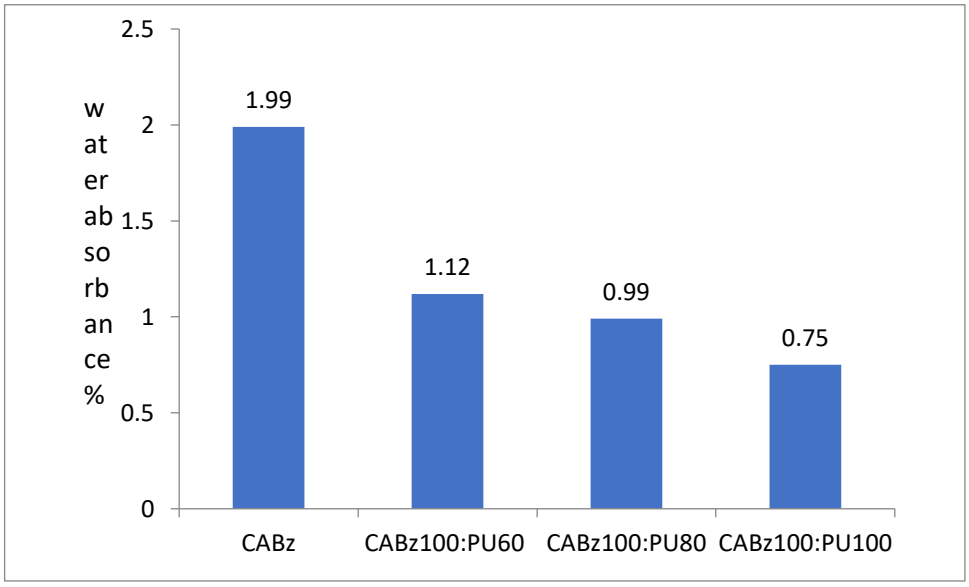

Figure 6: The percentage of water adsorption analysis of monomer and its co-polymeric material.

Microscopic optical image studies

The concentration of polymeric material is clearly visible while looking in the microscope. Figure 7 clearly showed the impact of the polymer material to reduce the corrosion rate. The bare MS exhibits higher corrosion and their morphology is highly damaged due to corrosion. The morphology of coated plates clearly shows the less corrosive damage. The increasing polyurethane content reduces the corrosion rate. These findings recommend that the higher concentration of polyurethane with monomer acts as superior anti-corrosive agent. The above experiments suggests that incorporating more polyurethane component showing higher resistance to corrosion is highly recommended.

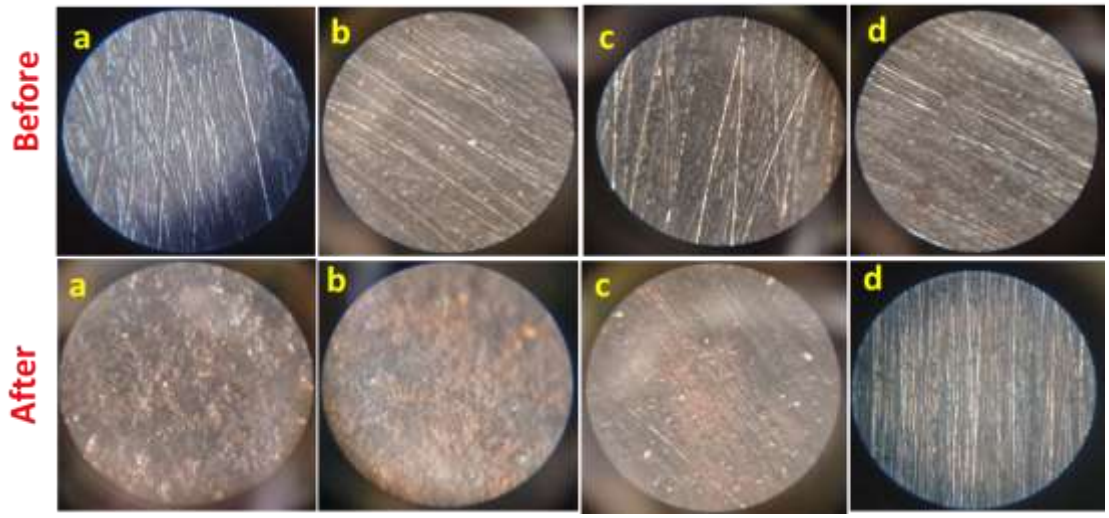

Figure 7: Microscopic images of mild steel after and before corrosion (a) blank, (b) APB:PU (100:60), (c) APB:PU (100:80) and (d) APB:PU (100:100).

Theoretical analysis

Density Functional Theory (DFT) is a powerful computational technique used in physics, chemistry, and materials science to study the electronic structure of atoms, molecules, and condensed phases[30]. Let's look at its chemical applications, which include comprehending chemical processes, surface science and catalysis, material sciences, homogeneous/heterogeneous reactions, chemical sensors, and electrochemical reactions[31]. Frontier molecular orbitals (FMOs) are formed by combining higher occupied molecular orbitals (HOMOs) and lower unoccupied molecular orbitals (LUMO). This FMO could help understand the molecule's electronic transition and electron distribution on the surface, therefore providing the polarity of the molecule.

The FMO orbital analysis of the synthesized monomer has been thoroughly investigated to gain insights into the reactivity and electronic distribution of the compound. The orbitals (HOMO and LUMO) can be observed in figure 8, clearly illustrating the intra-molecular charge distribution across the molecule. At the HOMO level, electrons are dispersed throughout the molecule, particularly in the benzacetamide group. This transformation could be attributed to the presence of a donor-acceptor system within the molecule. The amide functional group acts as the acceptor unit, while the toluene group at the other end serves as the donor, thereby facilitating the ICT of the molecule. Additionally, the energy levels of these orbitals can be utilized to calculate various parameters such as band gap, global hardness, global softness, electrophilicity index, and chemical potential. The values obtained for these parameters are presented in Table 2. A more negative chemical potential value and a more positive electrophilicity index indicate the monomer's polarity, a chemical property that could lead to the formation of more cross-linked bonds with polyurethane. These bonds have the potential to enhance other physical properties, as previously discussed (gel content and water adsorption), making them crucial for the development of anti-corrosive materials. The synthesized polymeric material resulting from this study exhibits improved activity, highlighting the chemical reactivity of the monomer and its contribution to the physical properties of the co-polymeric material.

Table 2: Data obtained from DFT studies

Compound Name	HOMO (eV)	LUMO (eV)	Band Gap (eV)	Chemical potential	Global Hardness	Global Softness	Electrophilicity Index
Monomer	-5.8556	-1.4748	4.3807	-3.6652	2.1903	0.2282	3.0365
Polymer	-5.0802	-1.0716	4.008	-3.0759	2.0042	0.2494	2.3602

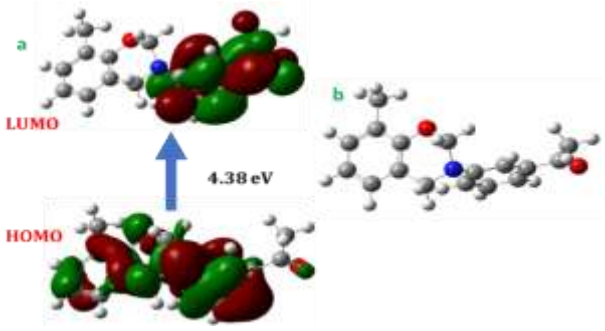

Figure 8: FMO analysis of synthesized monomer (a) and its optimized structure (b).

Molecular electrostatic mapping

Molecular Electrostatic Mapping, also known as Electrostatic Potential Maps or ESP Maps, offers a detailed view of the charge distribution within molecules. These maps help us to understand the regions of different charge of a molecule and predict how molecules interact with each other[32]. They are an excellent tool for viewing the charge distributions of molecules and gaining insights into charge-related characteristics and molecular behavior. This study involves overlaying the computed electrostatic potential energy data onto an electron density model generated from the Schrödinger equation. The resulting data is visually displayed by a color spectrum, with red denoting the lowest electrostatic potential energy value and blue signifying the highest[33]. Electrostatic potential maps are essential in predicting the behavior of complex molecules in organic chemistry, as well as in the study of molecular polarity, charge distribution, and interactions. To continue DFT research, the molecular electrostatic mapping is produced from the optimized structure and shown in figure 9. The red color electron may have been produced for the acetamide carbonyl oxygen, suggesting a higher electron content. On the other hand, the toluene component lacks electrons and appear green. The center-core component of the molecule, known as the benzoxazole group, is very pale-yellow, indicating that the oxygen and nitrogen molecules have a lower electron density. This observation via the DFT calculations, gives an idea of the molecule's polarity.

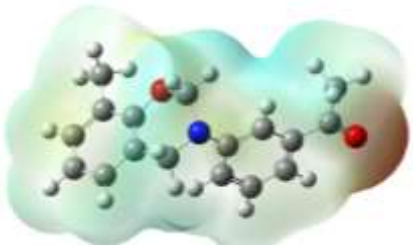

Figure 9: Molecular electrostatic mapping analysis of synthesized monomer molecule.

Conclusion

Various spectroscopic techniques such as NMR, FT-IR, and absorption spectroscopy were used to characterize the synthesized monomer. The polymer was made using high-temperature curing and the characterization results indicated the formation of the polymer under various reaction conditions. Additionally, the water absorption and gel content properties of both the monomer and polymeric materials were studied. Results confirmed that the monomer's properties were improved through polymerization, resulting in a increasing hydrophobic nature and strong gel content that contributed to a more cross-linked polymeric structure. These exceptional physical properties of the polymers demonstrated high resistance to mild steel corrosion, as shown by electrochemical studies. The electronic and chemical properties of the monomer were also investigated through DFT studies, which were in line with the corrosion results. This study suggests that both the monomer and its polymers have the potential to serve as effective anti-corrosive agents for mild steel.

ACKNOWLEDGMENT

I am thankful to the, Department of Chemistry, Thiruvalluvar Government Arts College,for providing all facilities for experimental work.

Conflict of interest

The authors declare no conflict of interest.

References

1. Chen, L.; Lu, D.; Zhang, Y. *Materials* **2022**, *15(6)*, 2023
2. Liu, C.; Revilla, R.I.; Liu, Z.; Zhang, D.; Li, X.; Terryn, H. *Corrosion Science* **2017**, *129*, 82–90
3. Ma, Q.; Tong, Z.; Wang, W.; Dong, G. *Appl. Surf. Sci.***2018**, *455*, 748–757
4. Ye, Y.; Liu, Z.; Liu, W.; Zhang, D.; Zhao, H.; Wang, L.; Li, X. *Chem. Engg. J.***2018**, *348*, 940–951
5. Jamrozik, A.; Barczewski, M.; Framski, G.; Baranowski, D.; Jakubowska, P.; Klapiszewski, L.; Jesionowski, T.; Voelkel A.; Strzemiecka, B. *Materials***2020**, *13(13)*, 2995
6. Bhushan, B. *Modern Tribology Handbook; CRC Press: Boca Raton, FL, USA*, **2000**; ISBN 978-0849384035
7. Artur Jamrozik, Mateusz Barczewski, Grzegorz Framski, Daniel Baranowski, Paulina Jakubowska, Tukasz Klapiszewski, Teofil Jesionowski, Adam Voelkel and Beata Strzemiecka*; Materials **2020**, 13(13), 2995; https://doi.org/10.3390/ma13132995*
8. Papavinasam, S. *Elsevier*, **2017**
9. Unueroh, U.; Omonria, G.; Efosa, O.; Awotunde, M. *Nigerian J. Technol.***2016**, *35(2)*, 317-320
10. Zhou, C.; Lin, J.; Lu, X.; Xin, Z. *RSC Adv.***2016**, *6*, 28428–28434
11. Sayed, M. M.; Abdel-Hakim, M.; Mahross, M. H.; Aly, K. I. *Sci. Rep.***2022**, *12*, 12878
12. Ren, S.; Cui, M.; Chen, X.; Mei, S.; Qiang, Y. *J. Colloid Interface Sci.***2022**, *628(B)*, 384–397
13. Reiss, G.; Schwob, J.M.; Guth, G.; Roche, M.; Lande B. *B.M. Culbertson, J.E. McGrath (Eds.), Advances in Polymer Synthesis, Plenum, New York*, **1985**, p. 27
14. Saiev, S.; Bonnaud, L.; Dubois, P.; Beljonne D.; Lazzaroni, R. *Polym. Chem.*, **2017**, *8*, 5988-5999
15. Thompson, S.; Stone, C. A.; Howlin, B. J.; Hamerton, I. *Polymers (Basel)***2018**, *10(11)*, 1250

16. Puozzo, H.; Saiev, S.; Bonnaud, L.; Winter, J. D.; Lazzaroni, R.; Beljonne,D. *Macromolecules*, **2022**, *55*, 10831-10841
17. Klfout, H. A.; Asiri, A. M.; Alamry K. A.; Hussein, M. A. *RSC Adv.*, **2023**, *13*, 19817-19835
18. Mingzhen Xu, Jiaqu Zhang, Bo Li, Zexu Fan, Lunshuai He, Effects of the Backbone's Structures on the Curing Behaviors and Properties of Phthalonitrile Containing Benzoxazine Rings, *Molecules*, ***2024,*** *29(23), 5637; https://doi.org/10.3390/molecules29235637*.
19. Casarino, A. F.; Bortolato, S. A.; Casis, N.; Estenoz, D. A.; Spontón,M. E. *European Polymer Journal*, **2023**, *182(2)*, 111722
20. Sriharshitha, S.; Krishnadevi, K.; Devaraju, S.; Srinivasadesikan, V.; Lee,S.-L.; *ACS Omega*, **2020**, *5(51)*, 33178–33185
21. Zhang, K.; Yua, X.; Kuo, S-W. *Polym. Chem.*, **2019**, *10*, 2387-2396
22. Periyasamy, T.; Asrafali, S. P.; Kim, S-C. *Polymers (Basel).***2023**, *15(4)*, 849
23. Takeichi, T.; Kawauchi, T.; Agag, T. *Handbook of Benzoxazine Resins***2011**, 378-387
24. Ganesh Naidu Gopu and Sofi Androse Joseph, Corrosion Behavior of Fiber-Reinforced Concrete - A Review Fibers, ***2022***, 10(5), 38; https://doi.org/10.3390/fib10050038
25. Ghazaleh Sadidi, Mahboobeh Azadi, Hossein Tavakoli, A new study on the effects of clay nanoparticles on the corrosion performance of Al-Si-Cu matrix composites in both acidic and alkaline solutions, *Materials*, ***2024***, 39, 109109, https://doi.org/10.1016/j.mtcomm.2024.109109
26. Salwa.M. El-Mesallamy, Preparation, characterization and evaluation of polybenzoxazine thermoset/clay nanocomposites for metal coating, *Egyptian Journal of Petroleum*, ***2019***, 28(3), 253-260, https://doi.org/10.1016/j.ejpe.2019.05.003
27. Lu, X.; Liu, Y.; Zhou, C.; Zhanga, W.; Xin, Z. *RSC Adv.,***2016**, *6*, 5805-5811
28. Kavitha, R.; Nirmala, S.; Nithyabalaji R.; Sribalan, R. *J. Mol. Struct.***2020**, *1204*, 127508
29. Phalak, G. A.; Patil, D. M.; Mhaske, S. T. *Eur. Polym. J*., **2017**, *88*, 93-108
30. Yong-Kul Lee, Catalysts **2021**, *11(4)*, 454; https://doi.org/10.3390/catal11040454.
31. Nishat, S. S.; Hossain, Md. J.; Mullick, F. E.; Kabir, A.; Chowdhury, S.; Islam, S.; Hossain, M. *J. Phys. Chem. C*, **2021**, *125(24)*, 13158-13166
32. Suresh, H.; Remya, G. S.; Anjalikrishna, P. K. *WIREs Computational Molecular Science*, **2022***12(5)*
33. Lakshminarayan, S.; Jeyasingh, V.; Murugesan, K.; Selvapalam, N.; Dass, G. *Journal of Photochemistry and Photobiology*, **2021**, *6*.